Acta Crystallographica Section F
Structural Biology and Crystallization Communications
ISSN 1744-3091

Superoxide reductase from the syphilis spirochete *Treponema pallidum*: crystallization and structure determination using soft X-rays

Teresa Santos-Silva, José Trincão, Ana L. Carvalho, Cecília Bonifácio, Françoise Auchère, Isabel Moura, José J. G. Moura and Maria J. Romão*

REQUIMTE Departamento de Química, Faculdade de Ciências e Tecnologia, Universidade Nova de Lisboa, 2829-516 Caparica, Portugal

Correspondence e-mail: mromao@dq.fct.unl.pt

Received 8 August 2005
Accepted 12 September 2005
Online 20 October 2005

Superoxide reductase is a 14 kDa metalloprotein containing a catalytic non-haem iron centre [Fe(His)$_4$Cys]. It is involved in defence mechanisms against oxygen toxicity, scavenging superoxide radicals from the cell. The oxidized form of *Treponema pallidum* superoxide reductase was crystallized in the presence of polyethylene glycol and magnesium chloride. Two crystal forms were obtained depending on the oxidizing agents used after purification: crystals grown in the presence of $K_3Fe(CN)_6$ belonged to space group $P2_1$ (unit-cell parameters $a = 60.3$, $b = 59.9$, $c = 64.8$ Å, $\beta = 106.9^\circ$) and diffracted beyond 1.60 Å resolution, while crystals grown in the presence of Na_2IrCl_6 belonged to space group $C2$ ($a = 119.4$, $b = 60.1$, $c = 65.6$ Å, $\beta = 104.9^\circ$) and diffracted beyond 1.55 Å. A highly redundant X-ray diffraction data set from the $C2$ crystal form collected on a copper rotating-anode generator ($\lambda = 1.542$ Å) clearly defined the positions of the four Fe atoms present in the asymmetric unit by SAD methods. A MAD experiment at the iron absorption edge confirmed the positions of the previously determined iron sites and provided better phases for model building and refinement. Molecular replacement using the $P2_1$ data set was successful using a preliminary trace as a search model. A similar arrangement of the four protein molecules could be observed.

1. Introduction

Until recently, superoxide dismutases (SOD) were the only enzymes known to detoxify the superoxide anion (McCord & Fridovich, 1969; Fridovich, 1995). In 1999 a new defence mechanism against oxygen toxicity was reported for some anaerobic organisms and archaea, involving a non-haem iron protein, superoxide reductase (SOR; Jenney *et al.*, 1999). SOR is able to scavenge superoxide radicals from the cell by catalyzing the one-electron reduction of superoxide to hydrogen peroxide,

$$O_2^{\cdot -} + 2H^+ + \mathrm{SOR}\ (Fe^{2+}) \rightarrow H_2O_2 + \mathrm{SOR}\ (Fe^{3+}).$$

The active site of the enzyme consists of an iron centre with a square-pyramidal geometry coordinated by four equatorial histidines and one axial cysteine [Fe(His)$_4$Cys]. The superoxide radical binds to the reduced form of the Fe atom in the free axial position. Despite the presence of very similar active sites, the SOR family can be divided into three classes depending on the presence of an N-terminal domain (Rusnak *et al.*, 2002).

Members of class I (also called 2Fe-SORs) contain two domains, each harbouring a different type of metal centre. The catalytic domain contains the iron active site Fe(His)$_4$Cys. A short N-terminal rubredoxin/desulforedoxin-like domain (Archer *et al.*, 1995; Dauter *et*

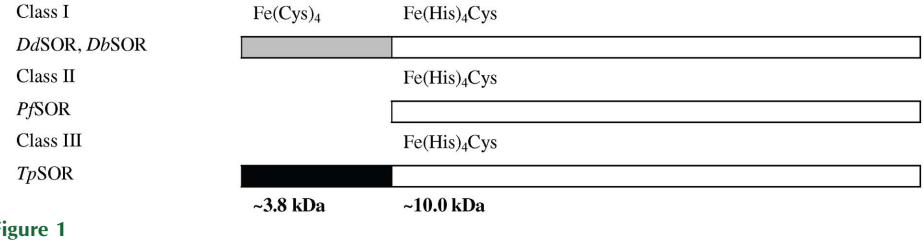

Figure 1
Classes of SOR.

Table 1
Data-processing statistics for the four data sets of oxidized *Tp*SOR.

Values in parentheses correspond to the highest resolution shell.

Data set	*Tp*SOR1	*Tp*SOR2	*Tp*SOR3	*Tp*SOR4
Space group	$P2_1$	$C2$		
Oxidizing agent	$K_3Fe(CN)_6$	Na_2IrCl_6		
Unit-cell parameters (Å, °)	a = 60.3, b = 59.9, c = 64.8, β = 106.90	a = 119.4, b = 60.01, c = 65.6, β = 104.90		
Source	ID14-2	In-house Cu $K\alpha$	BM14 peak	BM14 remote
Wavelength (Å)	0.933	1.542	1.739	1.033
No. of observed reflections	373462	581439	219096	366944
No. of unique reflections	58650	30190	28909	53059
Resolution limits (Å)	30.0–1.60 (1.66–1.60)	22.0–1.96 (2.07–1.96)	24.0–2.00 (2.11–2.0)	24.7–1.55 (1.63–1.55)
Redundancy	3.1 (2.2)	19.2 (18.1)	7.6 (7.6)	6.9 (5.4)
R_{sym}† (%)	7.9 (22.7)	8.2 (39.6)	4.5 (11.4)	4.3 (17.7)
Completeness (%)	99.7 (99.4)	94.2 (94.2)	95.0 (95.0)	82.4 (82.4)
$\langle I/\sigma(I)\rangle$	12.2 (4.2)	8.8 (1.9)	9.6 (5.3)	8.8 (4.3)
Mosaicity (°)	0.25	0.6		
R_{ano}‡ (%)		2.7 (10.4)	3.0 (5.6)	

† $R_{sym} = 100 \times \sum|I_i(j) - \langle I(j)\rangle|/\sum I_i(j)$, where $I_i(j)$ is the ith measurement of reflection j and $\langle I(j)\rangle$ is the overall weighted mean of j measurements. ‡ $R_{ano} = 100 \times \sum|I_{hkl}(+) - I_{hkl}(-)|/\sum[I_{hkl}(+) + I_{hkl}(-)]$.

al., 1992) harbours an $Fe(Cys)_4$ centre. Members of classes II and III (1Fe-SORs) contain only one iron active site, but differ in terms of domain structure. Members of class II (1Fe short-chain SORs) are characterized by possessing only the catalytic domain, while in members of class III (1Fe long-chain SORs) an additional N-terminal domain is present, but with no metal site (Fig. 1).

Crystal structures are available for the class I *Desulfovibrio desulfuricans* SOR (*Dd*SOR; Coelho *et al.*, 1997) and *Desulfoarculus baarsii* SOR (*Db*SOR; Adam *et al.*, 2004) and for the class II *Pyrococcus furiosus* SOR (*Pf*SOR; Yeh *et al.*, 2000). In the two classes, SOR molecules are organized as functional homodimers with a similar overall architecture.

Superoxide reductase isolated from *Treponema pallidum* (*Tp*SOR), the pathogenic bacterium responsible for syphilis, is also a functional homodimer of two 14 kDa subunits. *Tp*SOR is the first representative of a class III SOR to be structurally characterized. By amino-acid sequence comparison and analysis of the three-dimensional structures available, structural homology in the catalytic domain is expected. However, with respect to the N-terminal domain, the absence of a structural iron centre raises questions about its fold stabilization and physiological role. We expect that the structure of *Tp*SOR will shed some light on this structural divergence among the three classes, providing additional insight into the mechanism of superoxide detoxification.

2. Materials and methods

2.1. Purification and crystallization

T. pallidum superoxide reductase was cloned, overexpressed and purified to homogeneity according to the procedure previously described by Jovanovic *et al.* (2000). After overexpression of the gene in *Escherichia coli*, crude extracts were injected onto an anion-exchange column (DEAE-Sepharose, Pharmacia) followed by gel-filtration chromatography (Sephadex G75, Amersham Biosciences). Pure fractions were pooled and concentrated using an Amicon concentrator equipped with a YM3 membrane. A mixture of the reduced and oxidized states was obtained under these conditions.

The complete oxidation of superoxide reductase was achieved by addition of 50 m*M* $K_3Fe(CN)_6$ to the protein solution. EPR and FTIR studies indicated the formation of an adduct between ferricyanide and the protein iron centre (Auchère *et al.*, 2003). In order to prevent formation of this complex, Na_2IrCl_6 was used as an alternative oxidizing agent. The two purification batches prepared with the different oxidants were used for crystallization.

Crystallization trials of the oxidized form of *Tp*SOR have been prepared using the hanging-drop vapour-diffusion method in 24-well Linbro plates. Preliminary crystallization conditions were screened at 277 and 293 K using an in-house-modified version of the sparse-matrix method of Jancarik & Kim (1991) in combination with Crystal Screen and Crystal Screen 2 from Hampton Research. The presence of different oxidants in the protein solution yielded two distinct crystal forms under similar crystallization conditions.

The first crystallization experiments were set up using a 10 mg ml^{-1} solution of *Tp*SOR in 10 m*M* Tris–HCl pH 7.8 with an excess of $K_3Fe(CN)_6$. 2 µl of this protein solution was mixed with the same volume of a solution containing 25%(*w*/*v*) PEG 3350, 0.2 *M* magnesium chloride and 0.1 *M* Tris–HCl pH 7.0. Blue plate-shaped crystals grew within 12 d to their maximum size, 0.15 × 0.05 × 0.05 mm, both at 277 and 293 K. Further crystallization experiments were performed with the protein treated with Na_2IrCl_6 and new crystals were grown by mixing equal amounts of SOR (10 mg ml^{-1} in 20 m*M* Tris–HCl pH 7.6, treated with Na_2IrCl_6) and the crystallization solution described above. Crystals of similar morphology were obtained. Sodium ascorbate has been used to fully reduce SOR; crystallization attempts have been unsuccessful so far.

The two crystal forms of the oxidized *Tp*SOR were soaked for a few seconds in a modified crystallization solution containing 20%(*v*/*v*) glycerol and flash-cooled in a nitrogen stream at 100 K for data collection.

2.2. Data collection and processing

Preliminary crystal characterization was performed using Cu $K\alpha$ X-ray radiation from an Enraf–Nonius rotating-anode generator operated at 5 kW with a MAR Research image-plate detector.

The diffraction experiments showed that the two crystal forms belong to two different monoclinic space groups. The presence of $K_3Fe(CN)_6$ in the crystallization conditions produced crystals in space group $P2_1$, with unit-cell parameters a = 60.3, b = 59.9, c = 64.8 Å, β = 106.9°. In the presence of Na_2IrCl_6 a distinct crystal form was obtained belonging to space group $C2$, with unit-cell parameters a = 119.4, b = 60.1, c = 65.6 Å, β = 104.9°.

Four different data sets were collected from the $P2_1$ and the $C2$ crystals and are here designated *Tp*SOR1–4.

A complete data set from a $P2_1$ crystal (*Tp*SOR1) was collected at beamline ID14-2 at the European Synchrotron Radiation Facility (ESRF, Grenoble, France) using a 165 mm MAR CCD detector. At a wavelength of 0.933 Å, these crystals diffracted beyond 1.6 Å resolution.

Three complete data sets were collected from the *C*2 crystal form. *Tp*SOR2 data were measured using the in-house copper rotating-anode generator described above. A very highly redundant data set was collected to beyond 1.9 Å resolution. A total of 970° of 1° oscillations were collected in approximately 72 h. *Tp*SOR3 and *Tp*SOR4 data were from a MAD experiment at the iron edge. The experiment was performed at the tunable-wavelength beamline BM14 of the ESRF. *Tp*SOR3 data were collected at the iron absorption peak (1.739 Å) and *Tp*SOR4 data were collected at 1.033 Å, a high-energy remote wavelength.

Data sets *Tp*SOR1 and *Tp*SOR2 were processed using the programs *MOSFLM* (Leslie, 1992) and *SCALA* (Kabsch, 1988) from the *CCP*4 suite (Collaborative Computational Project, Number 4, 1994). Data sets *Tp*SOR3 and *Tp*SOR4 were processed using the *HKL*2000 package (Otwinowski & Minor, 1997). Data-collection and processing statistics are presented in Table 1.

2.3. Structure solution

The Matthews coefficient (Matthews, 1968) calculated for the two crystal forms ($P2_1$ and *C*2) suggests the presence of four molecules in the asymmetric unit, with a solvent content of ∼43%.

Considering the high sequence homology between all members of this family, in particular in the catalytic domain, one would expect that Patterson search methods should give a solution from the available structures of class I and class II SOR. Attempts were carried out using search models of all available structures and the data from $P2_1$ crystals. Search models were generated with whole monomers, dimers, truncated domains and polyalanines, but to no avail. Different programs were used in these trials to obtain a molecular-replacement solution, including *MOLREP* (Vagin & Teplyakov, 1997), *AMoRe* (Navaza, 1994), *Beast* (Read, 2001), *Phaser* (Storoni *et al.*, 2004) and *CNSsolve* (Brünger *et al.*, 1998).

A second approach to structure determination was carried out taking advantage of the presence of anomalous scatterers in the native protein. The anomalous signal arising from the four Fe atoms present in the asymmetric unit, each belonging to one of the SOR molecules, was used to solve the structure. SAD and MAD experiments were performed using the recently grown *C*2 crystals.

In-house Cu $K\alpha$ radiation has been used to solve the structure of proteins containing anomalous scatterers (SAD; Dauter *et al.*, 1999; Weiss *et al.*, 2001). The major requirement for a SAD experiment to succeed is a highly redundant data set that enhances the poor anomalous signal of the scatterers at the measured wavelength (1.54 Å), far from the scatterers absorption edge. The data-collection strategy for the *Tp*SOR2 data set fulfilled this requirement. 970° of data were collected (1° oscillations), yielding an overall completeness of 94.2% and a redundancy of 19.2 (Table 1).

Anomalous difference Patterson maps calculated with the *Tp*SOR2 data set clearly showed the cross-vectors between the four Fe atoms in the asymmetric unit (Fig. 2).

The iron substructure was solved using *autoSHARP* (de La Fortelle & Bricogne, 1997), which identified the position of the four iron sites. These sites were used to calculate phases, with an FOM of 0.38. *autoSHARP* performed density modification but the phases obtained yielded a poor electron-density map that was not good enough to build a model (FOM after density modification was 0.40).

In order to improve the phases, a MAD data set was collected using synchrotron radiation. As expected, an increase in the anomalous signal was observed for the *Tp*SOR3 data set collected at the iron absorption edge. The peaks in the anomalous difference Patterson maps calculated for the iron peak data set are in agreement with those determined with the in-house data, confirming the positions of the sites.

Electron-density maps calculated using the peak data set *Tp*SOR3 are of much better quality and have been used for model building and refinement (the FOM before and after density modification was 0.55 and 0.66, respectively).

Using the *Tp*SOR preliminary model of the dimer built with the MAD data, new attempts to find a molecular-replacement solution using the $P2_1$ data were successful. *Phaser* (Storoni *et al.*, 2004) found

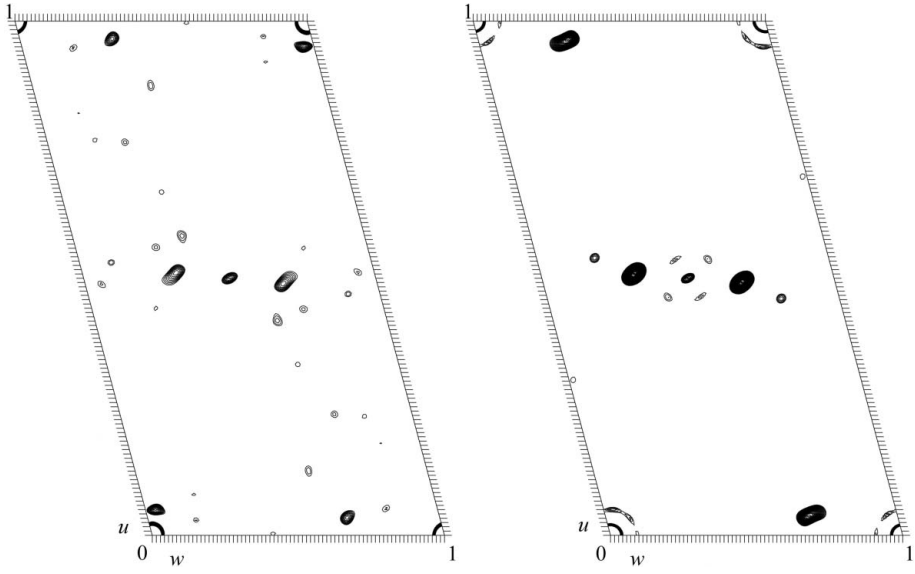

Figure 2
Harker section ($v = 0$) of the anomalous difference Patterson map (one unit cell is represented) contoured at 2σ. On the left side of the picture the Patterson function was calculated with the anomalous differences of the *Tp*SOR2 data set; on the right side a simulated Patterson map was calculated using the refined coordinates of the iron sites, determined with the *Tp*SOR3 data set. The figure was created using *CNSsolve* (Brünger *et al.*, 1998).

a solution with an LLG value of 1790 and a *Z*-score value of 14.9 for the rotation function and 47.8 for the translation function. After rigid-body refinement the FOM was 0.47. Electron density shows clear solvent boundaries for the four SOR molecules and *ARP*/*wARP* (Perrakis *et al.*, 1999) successfully traced most of the model ($R_{\rm factor}$ = 26.0%).

3. Results and discussion

T. pallidum superoxide reductase has been crystallized in two distinct crystal forms depending on the oxidant agent used after purification. The presence of four molecules in the asymmetric unit is common to both forms as suggested by the Matthews coefficient.

The arrangement of the four molecules should be analogous to the functional dimers observed in the class I and II SOR structures. The self-rotation function of the *C*2 crystals calculated using *POLARRFN* (Collaborative Computational Project, Number 4, 1994) shows four relevant peaks in the $\kappa = 180^\circ$ section (Fig. 3). The two peaks at $\varphi = 180^\circ$ [(136.8, 180, 180) and (46.4, 180, 180)] correspond to two twofold NCS axes and are related by 90°. The peaks at $\varphi = 90^\circ$ are derived from the crystallographic twofold axis. The asymmetry of these peaks indicates the presence of a third NCS axis nearly parallel to the crystallographic axis. This NCS axis is responsible for an extra peak in the anomalous difference Patterson map at $u = w = 0.5$ (Fig. 2). Based on these results, we can conclude that the four molecules are arranged as two functional dimers related by an NCS axis roughly parallel to the *b* axis of the unit cell. Two other NCS axes, about 45° away from this axis, relate the monomers of each functional dimer.

The positions of the iron sites were found using data collected using an in-house rotating copper-anode generator. The anomalous signal for this data set was small ($R_{\rm ano}$ = 2.7%, $R_{\rm merge}$ = 8.2%), yielding poor phases. The anomalous differences are larger in the data set collected at the iron absorption peak ($R_{\rm ano}$ = 3.0%, $R_{\rm merge}$ = 4.5%), providing useful phases for model building and refinement.

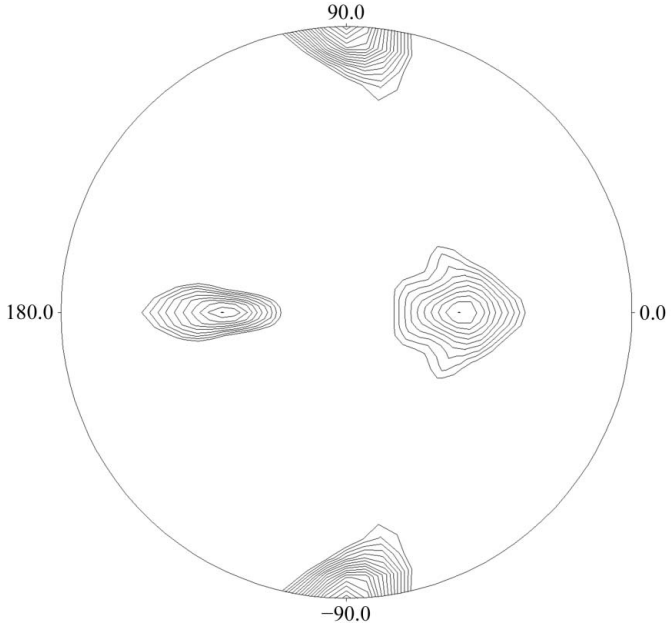

Figure 3
$\kappa = 180^\circ$ section of the self-rotation function calculated using the *Tp*SOR4 data set of the *C*2 crystals. The calculation was performed using data between 15 and 4.5 Å resolution, with a search radius of 15 Å. The four molecules in the asymmetric unit are arranged as a dimer of homodimers. Each monomer is related to its partner by a twofold NCS axis to form the functional dimer observed in the other SOR classes. The two peaks at $\varphi = 180^\circ$ are originated by these two axes. The NCS axis that relates the two functional dimers is nearly parallel to the crystallographic twofold axis and creates a distortion in the peaks at $\varphi = 90^\circ$. This figure was prepared using the program *POLARRFN* (Collaborative Computational Project, Number 4, 1994).

Even though the sequence similarities among the three classes suggested very similar structures, all attempts to solve the structure by molecular replacement were unsuccessful. Small differences in the orientation of the monomers in the functional dimers of each class may explain why the dimer did not work as a search model. However, this does not account for the failure using monomers.

When the *Tp*SOR dimer was employed as a search model for molecular replacement, a clear solution was found using the $P2_1$ data. The electron density obtained shows an overall arrangement of the molecules in the asymmetric unit similar to that observed in the C2 crystals.

The *Tp*SOR structure will undoubtedly provide valuable information for understanding of the divergence between the three classes of SOR and in particular the mechanism of oxygen detoxification.

This work was supported in part by Fundação para a Ciência e Tecnologia, SFRH/BD/6358/2001 TSS, BPD-9444/2002 (JT). The authors would like to thank Dr Hassan Belrhali for his help during synchrotron data collection at beamline BM14 at the ESRF, Grenoble, France. We would like to dedicate this work to the memory of Frank Rusnak.

References

Adam, V., Royant, A., Nivière, V., Molina-Heredia, F. P. & Bourgeois, D. (2004). *Structure*, **12**, 1729–1740.
Archer, M., Huber, R., Tavares, P., Moura, I., Moura, J. J. G., Carrondo, M. A., Sieker, L. C., LeGall, J. & Romão, M. J. (1995). *J. Mol. Biol.* **251**, 690–702.
Auchère, F., Raleiras, P., Benson, L. M., Yu, S., Tavares, P., Moura, J. J. G., Moura, I. & Rusnak, F. (2003). *Inorg. Chem.* **42**, 938–940.
Brünger, A. T., Adams, P. D., Clore, G. M., DeLano, W. L., Gros, P., Grosse-Kunstleve, R. W., Jiang, J.-S., Kuszewski, J., Nilges, M., Pannu, N. S., Read, R. J., Rice, L. M., Simonson, T. & Warren, G. L. (1998). *Acta Cryst.* D**54**, 905–921.
Coelho, A. V., Matias, P. M., Fulop, V. & Carrondo, M. A. (1997). *J. Biol. Inorg. Chem.* **2**, 680–689.
Collaborative Computational Project, Number 4 (1994). *Acta Cryst.* D**50**, 760–763.
Dauter, Z., Dauter, M., de La Fortelle, E., Bricogne, G. & Sheldrick, G. M. (1999). *J. Mol. Biol.* **289**, 83–92.
Dauter, Z., Sieker, L. C. & Wilson, K. S. (1992). *Acta Cryst.* B**48**, 42–59.
Fridovich, I. (1995). *Annu. Rev. Biochem.* **64**, 97–112.
Jancarik, J. & Kim, S.-H. (1991). *J. Appl. Cryst.* **24**, 409–411.
Jenney, F. E. Jr, Verhagen, M. F., Cui, X. & Adams, M. W. (1999). *Science*, **286**, 306–309.
Jovanovic, T., Ascenso, C., Hazlett, K. R., Sikkink, R., Krebs, C., Litwiller, R., Benson, L. M., Moura, I., Moura, J. J. G., Radolf, J. D., Huynh, B. H., Naylor, S. & Rusnak, F. (2000). *J. Biol. Chem.* **275**, 28439–28448.
Kabsch, W. (1988). *J. Appl. Cryst.* **21**, 916–924.
La Fortelle, E. de & Bricogne, G. (1997). *Methods Enzymol.* **276**, 472–494.
Leslie, A. G. W. (1992). *Jnt CCP4/ESF–EAMCB Newsl. Protein Crystallogr.* **26**.
McCord, J. M. & Fridovich, I. (1969). *J. Biol. Chem.* **244**, 6049–6055.
Matthews, B. W. (1968). *J. Mol. Biol.* **33**, 491–497.
Navaza, J. (1994). *Acta Cryst.* A**50**, 157–163.
Otwinowski, Z. & Minor, W. (1997). *Methods Enzymol.* **276**, 307–326.
Perrakis, A., Morris, R. & Lamzin, V. S. (1999). *Nature Struct. Biol.* **6**, 458–463.
Read, R. J. (2001). *Acta Cryst.* D**57**, 1373–1382.
Rusnak, F., Ascenso, C., Moura, I. & Moura, J. J. G. (2002). *Methods Enzymol.* **349**, 243–258.
Storoni, L. C., McCoy, A. J. & Read, R. J. (2004). *Acta Cryst.* D**60**, 432–438.
Vagin, A. & Teplyakov, A. (1997). *J. Appl. Cryst.* **30**, 1022–1025.
Weiss, M., Sicker, T. & Hilgenfeld, R. (2001). *Structure*, **9**, 771–777.
Yeh, A. P., Hu, Y., Jenney, F. E. Jr, Adams, M. W. & Rees, D. C. (2000). *Biochemistry*, **39**, 2499–2508.